Ionic Conductivity of Nanostructured Hybrid Materials Designed from Imidazolium Ionic Liquids and Kaolinite

Sadok Letaief, Thomas Diaco, Wendy Pell, Serge I. Gorelsky, and Christian Detellier*

Centre for Catalysis Research and Innovation and Department of Chemistry, University of Ottawa, 10 Marie Curie, Ottawa, Ontario, K1N6N5, Canada

Received March 22, 2008. Revised Manuscript Received July 4, 2008

Highly nanostructured hybrid materials were prepared by the intercalation into the interlayer spaces of kaolinite of ionic liquids based on imidazolium derivatives. Their structure, thermal behavior, and composition were characterized by a range of methods, including X-ray diffraction, solid-state NMR, thermal gravimetric analysis, and elemental analysis. Measurements of their electrical conductivity were carried out by impedance spectroscopy in the temperature range 23−250 °C. Three imidazolium derivatives were used: 1-methyl 3-propyl imidazolium bromide (Im-1), 1-methyl 3-(2-chloroethyl) imidazolium cloride (Im-2), and 1-methyl 3-(benzyl) imidazolium chloride (Im-3). The electrical conductivity depends on the size as well as on the structural organization of the salts into the interlayer space. In the case of the intercalates Im-1-K and Im-2-K, the electrical conductivity measured at room temperature is about 2×10^{-5} S cm^{-1}. This value varies with temperature. The maximum of conductivity, 4×10^{-4} S cm^{-1}, was obtained in a relatively short-range of temperatures, between 160 and 200 °C. No conductivity could be measured in the case of Im-3-K. An optimization of the structures of the three nanohybrid materials was performed using the PM6 semiempirical method. Alternating channels of organic cations and halide anions are formed in the cases of Im-1-K and Im-2-K, leading to the observed ionic conductivity behavior. In the presence of a bulkier substituent of the imidazolium ring, such as in Im-3-K, the anionic channels are blocked by the substituent, resulting in the absence of conductivity. To the best of our knowledge, this is the first report of electrical conductivity displayed by an interlayer modification of kaolinite.

Introduction

Nanohybrid materials prepared by the nanoscale incorporation of organic moieties into the interlayer spaces of layered inorganic hosts have received considerable attention in the past decade.[1] These materials combine the structural and textural properties of the host matrix with the chemical functionality of the organic guest.[2]

Among these nanohybrid materials, organo-clays constitute a versatile area of investigation, which is due in particular to the availability of natural clay minerals and their ability to incorporate a large variety of functional molecules, including polymers.[3] Among the clay minerals, the smectite group, including montmorillonite, is the most studied because of its favorable characteristics, such as swelling ability and cationic exchange capacity.[4]

Kaolinite is one of the most abundant clay minerals on Earth.[5] It is a 1:1 layered dioctahedral aluminosilicate, characterized by the chemical composition $Al_2Si_2O_5(OH)_4$. The individual layers are linked together through hydrogen bonds between the aluminol groups of the octahedral sheet on one side, and the siloxane macrorings of the tetrahedral

* Corresponding author. E-mail: dete@uottawa.ca.

(1) (a) *Handbook of Layered Materials*; Aucherbach, S., Carrado, K. A., Dutta, P., Eds.; Marcel Dekker: New York, 2004. (b) *Functional Hybrid Materials*; Gómez-Romero, P., Sanchez, C., Eds.; Wiley-VCH: Weinheim, Germany, 2004. (c) Ruiz-Hitzky, E. *Chem. Rec.* **2003**, *3*, 88–100. (d) *Polymer-Clay Nanocomposites*; Pinnavaia, T. J., Beall, G. W. J., Eds. Wiley and Sons: West Sussex, U.K., 2000. (e) *Hybrid Organic−Inorganic Composites*; Mark, J. E., Lee, C. Y. C., Bianconi, P. A., Eds.; American Chemical Society Washington, D.C. 1995.

(2) (a) Colilla, M.; Darder, M.; Aranda, P.; Ruiz-Hitzky, E. *Chem. Mater.* **2005**, *17*, 708–715. (b) de Paul, S. M.; Zwanziger, J. W.; Ulrich, R.; Wiesner, U.; Spiess, H. W. *J. Am. Chem. Soc.* **1999**, *121*, 5727–5736. (c) Hagrman, P. J.; Hagrman, D.; Zubieta, J. *Angew. Chem., Int. Ed.* **1999**, *38*, 2639–2684. (d) Wang, Z.; Pinnavaia, T. J. *Chem. Mater.* **1998**, *10*, 1820–1826. (e) Gomez-Romero, P.; Lira-Cantu, M. *Adv. Mater.* **1997**, *9*, 144–147. (f) Schubert, U.; Huesing, N.; Lorenz, A. *Chem. Mater.* **1995**, *7*, 2010–27. (g) Lao, H.; Latieule, S.; Detellier, C. *Chem. Mater.* **1991**, *3*, 1009–1011.

(3) (a) Ruiz-Hitzky, E.; Van Meerbeeck, A. In *Handbook of Clay Science*; Bergaya, F., Theng, B. K. G., Lagaly, G., Eds.;Elsevier: Amsterdam, 2006. (b) Lagaly G.; Ogawa, M.; Dekany, I. Clay Mineral Organic Interactions. In *Handbook of Clay Science, Developments in Clay Science, 1*; Bergaya, F., Theng, B. K. G., Lagaly, G., Eds.; Elsevier: Amsterdam, 2006; Chapter 7.3. (c) *Organoclay Complexes and Interactions*; Yariv, S., Cross, H., Eds.; Marcel Dekker: New York, 2002.

(4) (a) Szabo, T.; Szekeres, M.; Dekany, I.; Jackers, C.; De Feyter, S.; Johnston, C. T.; Schoonheydt, R. A. *J. Phys. Chem. C.* **2007**, *111*, 12730–12740. (b) Mehta, G. K.; Mark, J.; Lee, J. W.; Kotov, N.; Linderman, J. J.; Takayama, S. *Adv. Funct. Mater.* **2007**, *17*, 2701–2709. (c) Haraguchi, K.; Takehisa, T.; Ebato, M. *Biomacromolecules.* **2006**, *7*, 3267–75. (d) Bottino, F. A.; Fabbri, E.; Fragala, I. L.; Malandrino, G.; Orestano, A.; Pilati, F.; Pollicino, A. *Macromolecules* **2003**, *24*, 1079–1084. (e) Gilman, J. W.; Jackson, C. L.; Morgan, A. B., Jr.; Manias, E.; Giannelis, E. P.; Wuthenow, M.; Hilton, D.; Phillips, S. H. *Chem. Mater.* **2000**, *12*, 1866–1873. (f) Lee, A.; Lichtenhan, J. D. *J. Appl. Polym. Sci.* **1999**, *73*, 1993–2001. (g) Ajjou, A. N.; Harouna, D.; Detellier, C.; Alper, H. *J. Mol. Catal., A* **1997**, *126*, 55–60. (h) Mercier, L.; Detellier, C. *Environ. Sci. Technol.* **1995**, *29*, 1318–23.

(5) (a) Murray, H. H. Kaolin Minerals: Their Genesis and Occurence. In *Reviews in Mineralogy, Hydrous Phyllosilicates*; Bailey, S. W., Ed.; Mineralogical Society of America: Chelsea, MI, 1991; Vol. 19, Chapter 4, pp 67−87. (b) *Kaolin Genesis and Utilization*; Murray, H. H., Bundy, W., Harvey, C., Eds.; The Clay Mineral Society: Boulder, CO, 1993.

10.1021/cm800758c CCC: $40.75
Published on Web 10/25/2008

sheets on the other side. They are linked also by the strong dipole interactions between the noncentrosymmetric layers.[6] Consequently, kaolinite has been described as nonexpandable for a long time, until it was shown in the early sixties that some polar molecules could indeed be intercalated in its interlayer spaces.[7] Kaolinite is widely used in industry for various purposes, for example, as paper or cosmetics additive, and in ceramics.[8] However, because its interlayer spaces are not easily accessible, its interlayer chemistry is much less developed than the one of the clay minerals from the smectite group, particularly montmorillonite.

Intercalation of various organic molecules into kaolinite has been reported on the basis of direct replacement of intercalated polar molecules or salts. Recently, ionic liquids were intercalated in kaolinite, forming highly nanostructured materials.[10] Kaolinite−polymer intercalated nanocomposites have also been reported. They were prepared principally on the basis of two methods: (i) the direct intercalation of the polymer in synergy with the displacement of a polar guest preintercalated in kaolinite;[11] (ii) the intercalation of a monomer by a displacement method followed by its polymerization in situ.[12] Several examples of covalent grafting of organic units on the interlayer aluminol surfaces were reported in the last fifteen years.[13]

Montmorillonite shows ionic electrical conductivity resulting mainly from the migration of interlayer cations and from the diffusion of surrounding water molecules.[14] In the case of nanocomposites obtained by intercalation and polymerization of organic monomers into the interlayer space of montmorillonite, the electrical conductivity is mainly related to charge delocalization, resulting in electronic conductivity.[14c,15]

Scheme 1. Chemical Structures of the Imidazolium Salts Used in the Preparation of the Kaolinite Nanohybrid Materials

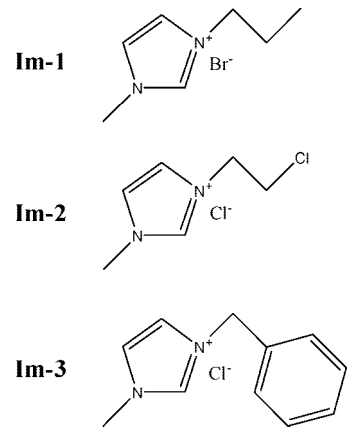

This paper reports electrical conductivity results of nanostructured materials prepared by intercalation of imidazolium salts into the interlayer space of kaolinite. The nanostructured materials were characterized by various techniques, and their electrical conductivities were measured at various temperatures (23−250 °C) using impedance spectroscopy.

To the best of our knowledge, this is the first report of electrical conductivity displayed by an interlayer modification of kaolinite.

Experimental Section

Materials. Well-crystallized kaolinite (KGa-1b; Georgia) was obtained from the Source Clay Repository of the Clay Minerals Society, Purdue University, West Lafayette, IN, USA. The purification of KGa-1b and the preparation of the dimethylsulfoxide-kaolinite intercalate (DMSO-K) were done according to previously published procedures.[10] 1-Methyl 3-propyl imidazolium bromide (Im-1), 1-methyl 3-(2-chloroethyl) imidazolium cloride (Im-2), and 1-methyl 3-(benzyl) imidazolium chloride (Im-3) (Scheme 1) were synthesized and characterized according to previously published procedures.[10b] Im-1 and Im-2 are liquids at room temperature, whereas Im-3 is a solid and its melting point is 33 °C.

Intercalation Reaction. (Scheme 2) The imidazolium salts were intercalated in kaolinite by a melt intercalation method using DMSO-K as starting material. Typically, 1.6 g of the imidazolium salt were added to 400 mg of DMSO-K (Im:DMSO-K = 4:1 w/w) at room temperature. The mixture was heated under a flow of nitrogen gas. The temperature was ramped up to 180 °C. During

(6) (a) Giese, R. F. *Clays Clay Miner.* **1978**, *26*, 51. (b) Giese, R. F. *Bull. Miner.* **1982**, *105*, 417.
(7) (a) Wada, K. *Am. Mineral.* **1961**, *46*, 78–91. (b) Ledoux, R. L.; White, J. L. *Science* **1964**, *143*, 244–246. (c) van Olphen, H. *An Introduction to Clay Colloid Chemistry*, 2nd ed.; Wiley-Interscience: New York, 1977.
(8) (a) Lopez-Galindo, A.; Viseras, C.; Cerezo, P. *Appl. Clay Sci.* **2007**, *36*, 51–63. (b) Ramalho, M. A. F.; Almeida, R. R.; Santana, L. N. L.; Lira, H. L.; Ferreira, H. C.; Neves, G. A. *Mater. Sci. Forum.* **2006**, 530–531. (c) Murray, H. H.; Kogel, J. E. *Appl. Clay Sci.* **2005**, *29*, 199–206. (d) Murray, H. H. *Clay Miner.* **1999**, *34*, 39–49.
(9) Ruiz-Hitzky, E; Aranda P.; Serratosa, J. M. Clay−Organic Interactions: Organoclay Complexes and Polymer−Clay Nanocomposites. In *Handbook of Layered Materials*; Aucherbach, S., Carrado, K. A., Dutta, P., Eds.; Marcel Dekker: New York, 2004; Chapter 3.
(10) (a) Letaief, S.; Detellier, C. *Clays Clay Min.* **2008**, *56*, 80–87. (b) Letaief, S.; Detellier, C. *J. Mater. Chem.* **2007**, *17*, 1476–1484. (c) Letaief, S.; Elbokl, T. A.; Detellier, C. *J. Colloid Interface Sci.* **2006**, *302*, 254–258. (d) Letaief, S.; Detellier, C. *J. Mater. Chem.* **2005**, *15*, 4734–4740.
(11) (a) Komori, Y.; Sugahara, Y.; Kuroda, K. *Chem. Mater.* **1999**, *11*, 3–6. (b) Tunney, J. J.; Detellier, C. *Chem. Mater.* **1996**, *8*, 927–935.
(12) (a) Elbokl, T. A.; Detellier, C. *J. Phys. Chem. Solids* **2006**, *67*, 950–955. (b) Matsumura, A.; Komori, Y.; Itagaki, T.; Sugahara, Y.; Kuroda, K. *Bull. Chem. Soc. Jpn.* **2001**, *74*, 1153–1158. (c) Sugahara, Y.; Satokawa, S.; Kuroda, K.; Kato, C. *Clays Clay Miner.* **1990**, *38*, 137–143. (d) Sugahara, Y.; Satokawa, S.; Kuroda, K.; Kato, C. *Clays Clay Miner.* **1988**, *36*, 343–348.
(13) (a) Letaief, S.; Detellier, C. *Can. J. Chem.* **2008**, *86*, 1–6. (b) Letaief, S.; Detellier, C. *Chem. Commun.* **2007**, 2613–2615. (c) Janek, M.; Emmerich, K.; Heissler, S.; Nüesch, R. *Chem. Mater.* **2007**, *19*, 684–693. (d) Gardolinski, J. E. F. C.; Lagaly, G. *Clay Miner.* **2005**, *40*, 547–556. (e) Gardolinski, J. E. F. C.; Lagaly, G. *Clay Miner.* **2005**, *40*, 537–546. (f) Murakami, J.; Itagaki, T.; Kuroda, K. *Solid State Ionics* **2004**, *172*, 279–282. (g) Itagaki, T.; Kuroda, K. *J. Mater. Chem.* **2003**, *13*, 1064–1068. (h) Brandt, K. B.; Elbokl, T. A.; Detellier, C. *J. Mater. Chem.* **2003**, *13*, 2566–2572. (i) Komori, Y.; Enoto, H.; Takenawa, R. J.; Hayashi, S; Sugahara, Y. S.; Kuroda, K. *Langmuir* **2000**, *16*, 5506–5508. (j) Tunney, J. J.; Detellier, C. *J. Mater. Chem.* **1996**, *10*, 1679–1685. (k) Tunney, J. J.; Detellier, C. *Clays Clay Miner.* **1994**, *42*, 552–560. (l) Tunney, J. J.; Detellier, C. *Chem. Mater.* **1993**, *5*, 747–748.
(14) (a) Letaief, S.; Aranda, P.; Ruiz-Hitzky, E. *Appl. Clay. Sci.* **2005**, *28*, 183–198. (b) Aranda, P.; Ruiz-Hitzky, E. *Appl. Clay. Sci.* **1999**, *15*, 119–135. (c) Galvan, J. C.; Jimenez-Morales, A.; Jimenez, R.; Merino, J.; Villanueva, A.; Crespin, M.; Aranda, P.; Ruiz-Hitzky, E. *Chem. Mater.* **1998**, *10*, 3379–3385.
(15) (a) Krishantha, D. M. M.; Rajapakse, R. M. G.; Tennakoon, D. T. B.; Dias, H. V. R. *Ionics* **2006**, *12*, 287–294. (b) Bandara, W. M. A. T.; Krishantha, D. M. M.; Perera, J. S. H. Q.; Rajapakse, R. M. G.; Tennakoon, D. T. B. *J. Compos. Mater.* **2005**, *39*, 759–775. (c) Castro-Acuna, C. M.; Fan, F. R.; Bard, A. J. *J. Electroanal. Chem. Interface Electrochem.* **1987**, *234*, 347–353.

Scheme 2. Intercalation Process of the Ionic Liquids in the Interlayer Space of Kaolinite

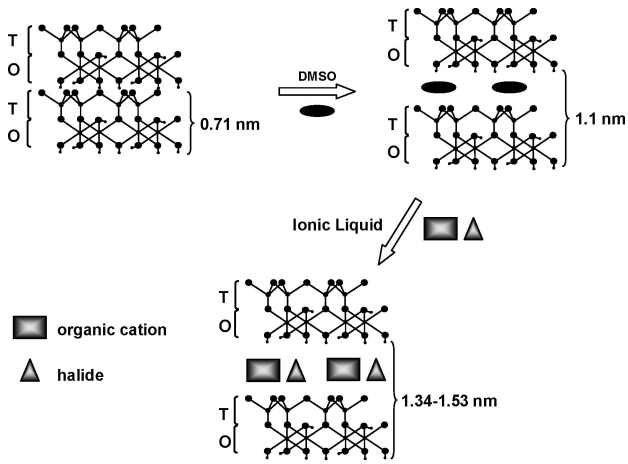

the heating process, the modified clay (DMSO-K) was in suspension in the ionic liquid. The suspension was then magnetically stirred at 180 °C during two hours under a flow of nitrogen. The excess molten salt was removed following four washing−centrifugation cycles using isopropanol. The recovered solid sample was dried at 60 °C overnight in air.

Characterization and Computational Details. X-Ray diffraction (XRD) patterns were obtained with a Philips PW 3710 instrument equipped with Ni-filtered and Cu Kα radiation (λ = 0.15418 nm) operating at 45 kV and 40 mA. Differential thermal analyses (DTA) and thermal gravimetric analyses (TGA) were recorded on a SDT 2960 Simultaneous DSC-TGA instrument with a heating rate of 3 °C min^{-1}. ^{13}C NMR CP/MAS spectra were collected on a Bruker AVANCE 500 NMR spectrometer operating at 125.77 MHz. The ^{13}C chemical shifts were referenced to tetramethylsilane (TMS) at 0 ppm using the high frequency signal of adamantane at 38.4 ppm as a secondary standard. Electrical conductivity behavior of the nanocomposites in the 23−250 °C temperature range was determined from ac impedance spectroscopy. Sputtered gold was used to cover the surface of the samples prepared as pellets (pressed at 4 ton/cm^2) to ensure electrical contact during impedance measurements. Impedance experiments were carried out with a Solartron 1255 HF frequency response analyzer coupled to Solartron Instrument SI 1287 Electrochemical Interface (100 mV applied signal in the 0.1−100 KHz frequency range). Z-PLOTW computer program was used for treatment of data and simulation of spectra.

The resistance of materials was determined as a function of temperature based on the equivalent electric circuit (EEC) methodology. Appropriate EECs, consisting of a series/parallel arrangements of resistors, capacitors and constant phase elements were determined and fit to the experimental data. The material resistance, R_B, was obtained from this analysis.[16]

The geometry optimizations of the nanohybrid materials were performed using the MOPAC2007 semiempirical package (version 7.072W). The atomic positions and cell dimensions were optimized with no constraints, using the PM6 semiempirical method. The eigenvector-following optimization scheme and the periodic boundary conditions with the tight energy and geometry convergence criteria were used.

(16) *Impedance Spectroscopy. Theory, Experiment and Applications*, 2nd ed.; Barsoukov, E., Macdonald, J. R., Eds.; Wiley-Interscience: Hoboken, NJ, 2005.

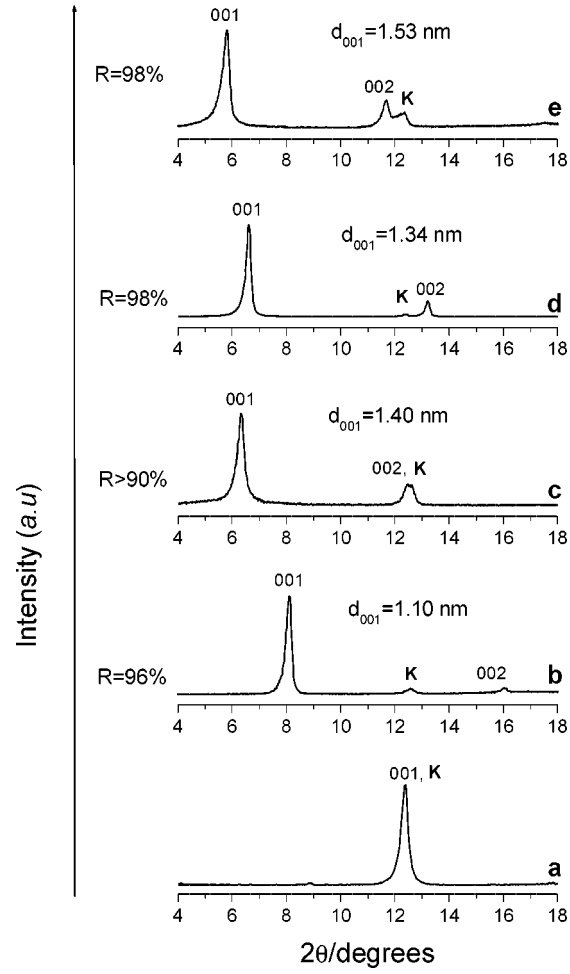

Figure 1. Oriented XRD patterns of (a) kaolinite (K), (b) kaolinite intercalated with DMSO (DMSO-K), (c) Im-1 (Im-1-K), (d) Im-2 (Im-2-K), and (e) Im-3 (Im-3-K).

Results and Discussion

The oriented XRD patterns of the pristine kaolinite (K), the starting materials (DMSO-K) and the nanohybrid materials recovered after the centrifugation, washing with isopropanol, and drying processes are shown in Figure 1. Upon intercalation of the imidazolium salt, the XRD patterns are characterized by an intense 001 reflection at 1.40 nm (Im-1-K) and at 1.34 nm (Im-2-K). Similarly, the 001 reflection of Im-3-K is observed at 1.53 nm. In all the cases, the d_{060} reflection of kaolinite remains at 1.49 Å (2θ = 62.3°), characteristic of a dioctahedral clay mineral, showing that the structure of the layers of kaolinite is maintained after the intercalation and the reaction processes. The intercalation ratios (obtained as an approximation, from the relative intensities of the d_{001} peaks of the intercalated and of the nonintercalated kaolinite) are 98% for Im-2-K and at least more than 90% for Im-1-K. In this case, one can only give a lower estimate of the ratio of intercalation because of the overlap of the 001 reflection of kaolinite at 0.71 nm with the 002 reflection of the nanohybrid at 0.70 nm. The reflection at 1.10 nm, characteristic of DMSO-K, was not observed after the reaction of the preintercalate with the ionic liquids. This is an indication that the intercalated DMSO molecules were replaced by the imidazolium ionic liquid during the intercalation process, which was fully confirmed

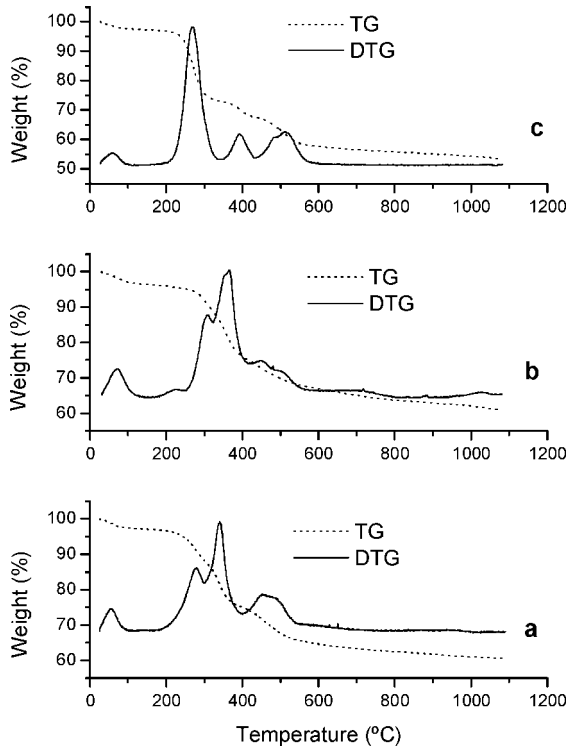

Figure 2. TG and DTG traces of Kaolinite intercalated with (a) Im-1 (Im-1-K), (b) Im-2 (Im-2-K), and (c) Im-3 (Im-3-K).

by ^{13}C MAS NMR. The two signals characteristic of DMSO intercalated in kaolinite at 42.9 and 43.8 ppm are completely absent in the NMR spectra of the nanohybrid materials.[10b]

The thermal gravimetric (TG) and differential thermal gravimetric (DTG) analysis traces are given in Figure 2 for Im-1-K, Im-2-K, and Im-3-K. The corresponding traces are given for kaolinite and DMSO-K in the Supporting Information (Figure S1). These data confirm the complete displacement of DMSO during the intercalation process. No weight loss was observed in the range 170−200 °C, which would be expected if DMSO molecules were still present in the intercalate. Compared to the starting material (DMSO-K), the nanohybrid materials exhibit improved thermal stability. The removal of the ionic liquids occurs in multiple steps at higher temperatures between 270 and 460 °C. The dehydroxylation of kaolinite is observed at 509, 504, and 513 °C, respectively, for Im-1-K, Im-2-K, and Im-3-K. These temperatures are close to the one characteristic of dehydroxylation of pure kaolinite at 515 °C, which confirms that the structure of kaolinite is not altered during the intercalation process.

The quantity of ionic liquid loaded by one structural unit of kaolinite was calculated from TG analysis (n_{TG}) and elemental analysis (n_{EA}). It was compared to theoretical values (n_{TH}) obtained taking into account the dimension of the organic cation, the Van der Waals radius of the corresponding halide. A very good agreement between the results obtained by the three methods supports the idea of an alternating cationic and anionic arrangement (see below, Computational Analysis). For all three nanohybrid materials, the number of ionic liquid molecules loaded by one kaolinite structural unit is close to 0.5. The similarity of the chemical structure of the ionic liquids could explain the similar loading

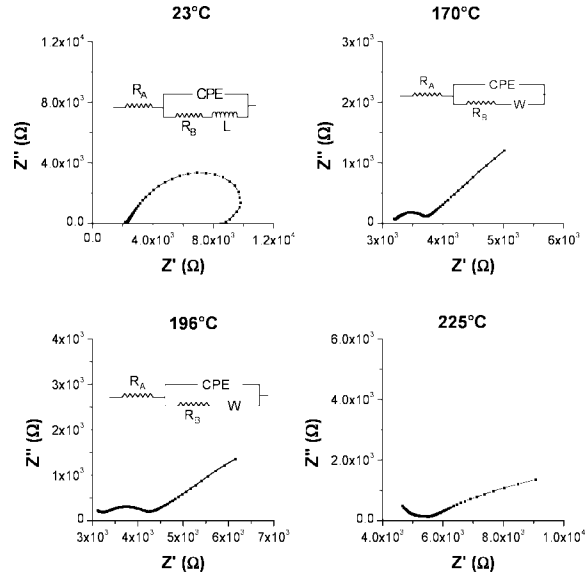

Figure 3. Nyquist plots and equivalent electric circuit of Im-1-K sample obtained at different temperature.

obtained. It was previously reported that the number of salt molecular units loaded by one kaolinite structural unit depends on the size of the organic cations. It is lower for larger salts.[10b]

Impedance Diagrams. The Nyquist plots of the Im-1-K sample obtained at various temperatures are presented in Figure 3. Typically, at room temperature (23 °C), the diagram is a distorted semicircle. The diameter of the semicircle is directly related to the resistance of the material. At higher temperatures (170−196 °C), the shapes of the Nyquist diagrams are different. They are composed of a semicircle at high frequencies, followed by a Warburg tail at low frequencies. For temperatures in the range of 200−225 °C, the impedance diagram exhibits predominantly a diffusion segment. Finally, for temperatures higher than 240 °C, the diagram is a dispersion of points, with an ill-defined Warburg tail. This is interpreted as a reactive system in which a progressive and continuous transformation is taking place. This phenomenon is related to the release and further decomposition of the imidazolium salts from the interlayer space of kaolinite, and is reminiscent of other reactive systems displaying similar behavior such as polypyrrole intercalated in montmorillonite and nontronite.[14a]

Evolution of Electrical Conductivity with Time. The electrical conductivity values σ of the nanohybrid materials were derived from the impedance diagrams. The conductivity was calculated from eq 1 where e is the thickness of the pellet in cm, A is the area of the pellet in cm^2, and R_B is the bulk resistance in ohms (see Experimental Section).

$$\sigma = (1/R_B)(e/A)\ \text{S cm}^{-1} \quad (1)$$

Figure 4 displays the evolution of the electrical conductivity with time for different sets of temperature, a different sample being used for each temperature. At room temperature (23 °C), the conductivity value remains constant during 60 min, around 1×10^{-5} S cm^{-1}. The lowest value obtained, corresponding to a sample heated to 120 °C, is 2×10^{-6} S cm^{-1}. At this temperature, the water adsorbed on the material is completely removed and thermal activation is sufficient

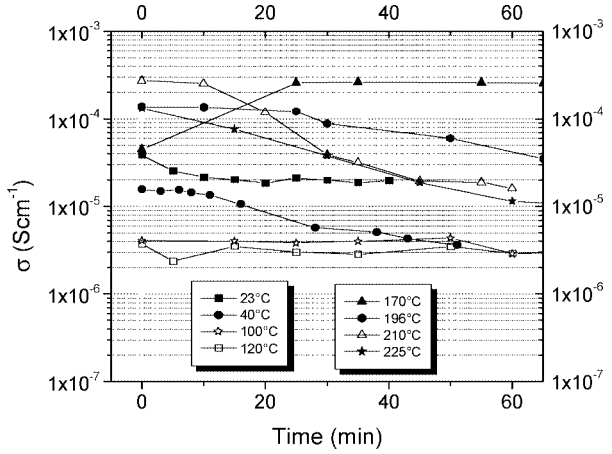

Figure 4. Electric conductivity versus time. Measurements were done at different temperatures for different samples of Im-1-K.

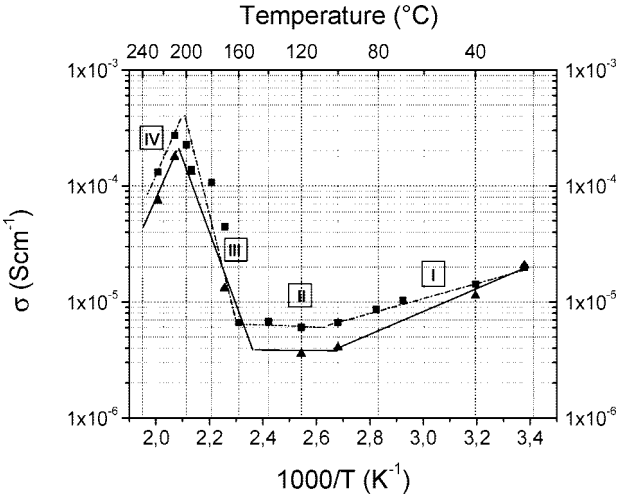

Figure 5. Evolution of the electric conductivity of Im-1-K with temperature. (■) Before each measurement, the same sample was maintained during 15 min at the desired temperature. (▲) For comparison, the data points resulting from a cross-section of Figure 4, at 15 min.

to ensure motion of the interlayer ionic species. A further increase in the temperature results in an increase in the ionic conductivity, as is observed for measurements done at 170, 196, and 210 °C. Measurements done at 170 °C show the highest conductivity. It is close to 3×10^{-4} S cm^{-1}. It remains constant for more than 90 min, whereas the values obtained at 196, 210, and 225 °C decrease with time due to a continuous decomposition of the material as it was observed by thermal analysis (see below).

Variation of Conductivity with Temperature. The electrical conductivity σ is given in Figure 5 as a function of 1000/T for the Im-1-K nanohybrid. In this case, the same sample was used throughout the full range of temperature, being heated 15 min at the desired temperature before each measurement. For comparison, a cross-section of Figure 4 after 15 min of heating each sample at the measurement temperature is also given in Figure 5. The fact that the sample treatment was different in the two cases, but resulted in similar conductivity results, points to the reproducibility of these experiments.

The Arrhenius plot reveals 4 zones described for Figure 5:

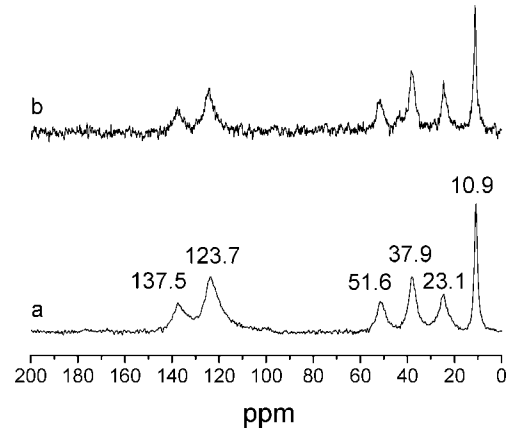

Figure 6. ^{13}C NMR CP/MAS spectra of (a) Im-1-K recovered after air drying at 60 °C and (b) Im-1-K heated at 170 °C for 90 min.

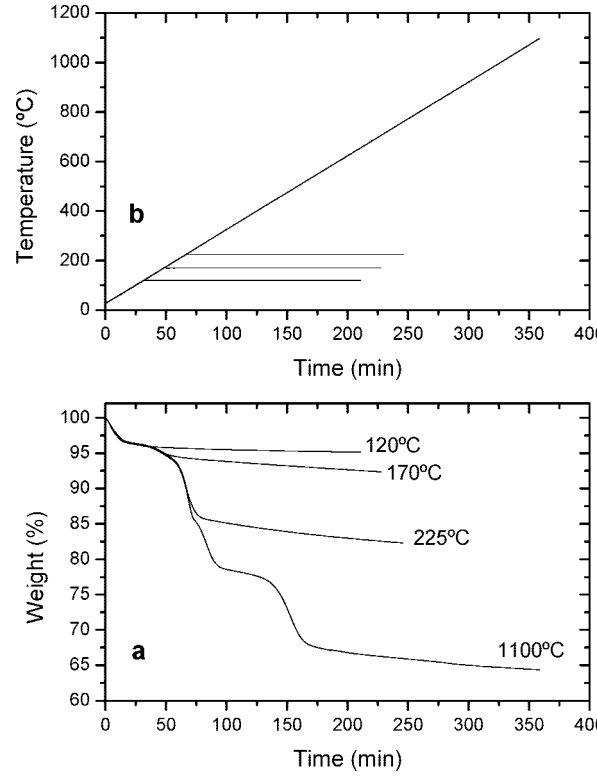

Figure 7. (a) TG traces of Im-1-K sample heated and maintained at different temperature. (b) Evolution of the temperature versus time.

Zone (I): The ionic conductivity decreases with temperature from 2×10^{-5} S. cm^{-1} at RT to 6×10^{-6} S. cm^{-1} at 100 °C. As shown by the thermal analysis data (see below, Figure 7), externally adsorbed water molecules are lost in that temperature range, which results in a continuous decrease of the observed conductivity until all the adsorbed water molecules have been removed. This is also in agreement with the ^{13}C NMR data, showing the unalteration of the imidazolium molecular structure up to 170 °C.

Zone (II): In the range 100 to 160 °C, the conductivity reaches a plateau, corresponding to a minimum of about 6×10^{-6} S. cm^{-1}. This corresponds to the actual contribution of the intercalated ionic liquid to the ionic conductivity. As observed from TG-DTG analysis, after complete removal of adsorbed water, no weight loss is observed in this range

of temperature. The sample does not undergo any structural transformation.

Zone (III): The electrical conductivity σ rises drastically from 6×10^{-6} S cm^{-1} to more than 2×10^{-4} S cm^{-1} within a short temperature range (160−200 °C) in which the mobility of the interlayer ions is strongly improved by thermal activation.

Zone (IV): As the temperature increases above 200 °C, a decrease of the conductivity is observed. It results from the release and the decomposition of the intercalated salts, in agreement with the decomposition observed from TG/DTG analysis (see Figures 2 and 7).

A similar behavior is observed when the sample is heated for a longer time before the conductivity measurements, in good agreement with the results displayed in Figure 4.

Figure 6a gives the ^{13}C CP/MAS NMR spectrum of the Im-1-K nanohybrid material dried at 60 °C. The expected signals of the imidazolium salt are observed, with an overlap of two signals in the olefinic region. To further test the thermal resistance of the intercalated organic salt, we recored the ^{13}C CP/MAS NMR spectrum after heating the material at 170 °C for 90 min. According to the TGA data, the organic salt has not yet been decomposed at that temperature. Only its partial loss is observed. This is nicely borne out by the NMR data. After heating at 170 °C for 90 min, the ^{13}C NMR spectrum is essentially identical to the one of the dry material, with an observed decrease of the signal-to-noise ratio.

Figure 7a gives the variation of the materials weight as a function of time after heating at a given temperature and keeping the sample at that temperature for a fixed period of time (3 h). Figure 7b illustrates the heating vs time process: the sample is slowly ramped to the desired temperature at a rate of 3 °C/min, then the temperature is held constant.

After being heated at 120 °C, water is lost, and the material is then thermally stable. Heating at 170 °C releases, slowly over time, a fraction of the organic material, but its molecular structure is conserved (see ^{13}C NMR data in Figure 6). This is essentially the behavior that can be observed at temperatures in the range of the sudden increase of conductivity with temperature increase. In that range, approximately from 160 to 200 °C (Figure 5), some organic material is removed, decreasing the packing of the organic cations and halogen anions in the interlayer space, consequently favoring the ionic mobility. At higher temperatures, a large fraction of the organic material is lost and begins to decompose. As a consequence, the conductivity falls considerably.

The conductivity was measured over time under the same conditions for the three nanohybrid materials. At room temperature, Im-1-K and Im-2-K give essentially the same result of conductivity, approximately 2×10^{-5} S. cm^{-1}, constant over time (Figure S2, Supporting Information). In strong contrast, no conductivity could be observed in the case of Im-3-K, in the range from room temperature to 200 °C.

Computational Analysis. To account for the conductivity behavior of Im-1-K and Im-2-K, and also to account for the lack of conductivity of Im-3-K, optimization of the structures of the nanohybrid materials was performed using the PM6 semiempirical method.

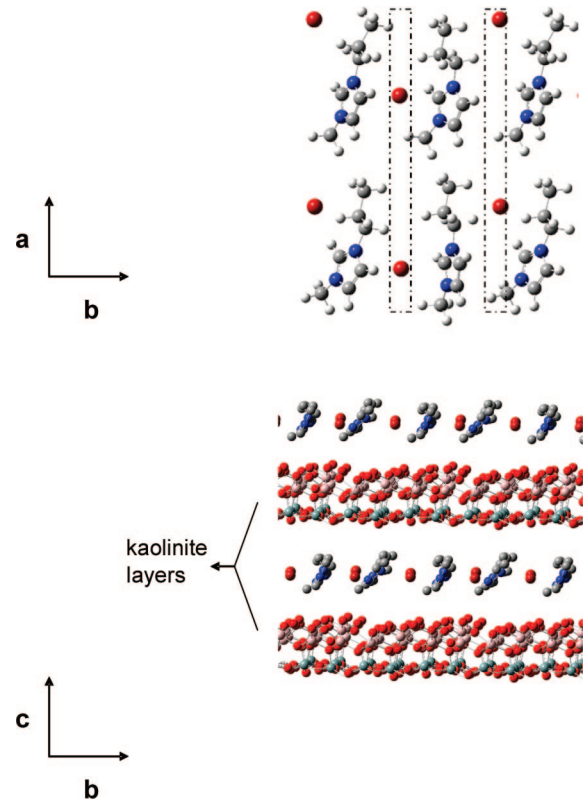

Figure 8. Calculated crystal structure of Im-1-K. For clarity, the top view (*a*, *b* plane) does not show kaolinite atoms and the side view (*c*, *b* plane) does not include the hydrogen atom. The dotted line is a representation of the tunnel structuration of the halide anions (see text).

The structure of kaolinite was optimized on the basis of previously published data,[17] and was in perfect agreement with the published results.[17a] The structures of Im-1-K and Im-3-K were optimized without any constraints (see Experimental Section) and are shown in Figures 8 and 9. The number of imidazolium halide ion pairs incorporated in the kaolinite structure was based of the experimentally determined loading of four ion pairs per eight kaolinite structural units.[10c] Then, periodic boundary conditions were used. The d_{001} values obtained from the computation, 1.39 and 1.49 nm for Im-1-K and Im-3-K, respectively, are remarkably close to the experimental values obtained from XRD, 1.40 nm and 1.53 nm, respectively. The interlayer distance is regulated by the tilt angle of the organic cation, which is approximately 60° with respect to the kaolinite internal surface. The imidazolium cations are aligned in a roughly parallel arrangement, with two slightly different structures. Tunnels are formed by the alignment of the imidazolium cations. The four walls of these truly nanohybrid tunnels are made of two imidazolium cations separated by 0.46 nm and of the two internal surfaces of kaolinite, the siloxane one and the aluminol one, separated by 1.40 nm. The tunnels, characterized by cross-sections of roughly 1.4×0.5 nm^2 are occupied by the bromide anions whose van der Waals diameter is 0.37 nm. Consequently, the movement of the anions in the tunnels of the interlayer spaces is not impeded

(17) (a) Benco, L.; Tunega, D.; Hafner, J.; Lischka, H. *J. Phys. Chem. B.* **2001**, *105*, 10812–10817. (b) Hobbs, J. D.; Cygan, R. T.; Nagy, K. L.; Schultz, P. A.; Sears, M. P. *Am. Mineral.* **1997**, *82*, 657–662.

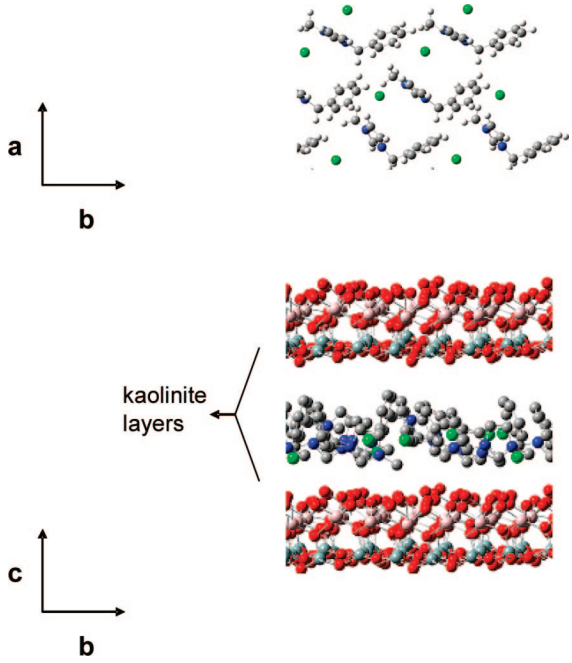

Figure 9. Calculated crystal structure of Im-3-K. For clarity, the top view (*a*, *b* plane) does not show kaolinite atoms and the side view (*c*, *b* plane) does not include the hydrogen atoms.

along the *a* axis (Figure 8). One can assume that the situation is similar in the case of Im-2-K in which the imidazolium structure is similar to Im-1-K and the chloride anion has a van der Waals diameter of 0.35 nm.

However, in strong contrast, in the structure of Im-3-K, whereas the imidazolium cations are also oriented in a roughly parallel arrangement, the phenyl rings of the benzyl substituants form a tetrahedral angle with respect to the imidazolium rings. This results in an arrangement that does not allow the formation of nanostructured tunnels as described in Im-1-K above (Figure 9). Consequently, the chloride anions are isolated in nanocavities surrounded in the *c*-direction by the two inorganic kaolinite surfaces and in the *a*- or *b*-direction by phenyl and imidazolium rings, which block the anion movements in the interlayer spaces.

Conclusion

Highly nanostructured hybrid materials are formed by the intercalation of imidazolium halide ionic liquids in the interlayer spaces of kaolinite. The imidazolium cations are aligned in a parallel arrangement forming alternating tunnels of organic cations and halide anions of 1.4 nm × 0.5 nm cross-sections. This structuration results in ionic conductivity which is highest in a relatively short temperature range, 160−200 °C. At higher temperatures, the conductivity drops dramatically due to the decomposition of the organic material and the resulting collapse of the structure. The conductivity behavior is highly dependent on the structure of the imidazolium derivatives. In the presence of bulkier substituents of the imidazolium ring, the halide channels are blocked by the substituents and no conductivity could be observed at any temperature. XRD, NMR, thermal and conductivity measurements are in excellent agreement with the nanohybrid materials structures obtained from PM6 semiempirical computations.

To the best of our knowledge, this is the first report of electrical conductivity displayed by an interlayer modification of kaolinite.

Acknowledgment. This work was financially supported by a Discovery Grant of the Natural Sciences and Engineering Research Council of Canada (NSERC) and by the Ontario Research and Development Challenge Fund (ORDCF). Dr Glenn A. Facey is thanked for recording the NMR spectra.

Supporting Information Available: Additional figures (PDF). This material is available free of charge via the Internet at http://pubs.acs.org.

CM800758C